RESEARCH IN PHARMACY AND MEDICINE
PHARMEDICINE JOURNAL

2024; 1(3):110-120. doi: 10.62482/pmj.16

Original Article

Amino Acid Supported Conductive Nanocomposite for Developing Flexible Electrode Material for Energy Storage

Sinem Ortaboy[1], Melisa Ogretici[1], Kibar Aras[2], Elif Caliskan Salihi[3]

[1]Istanbul University-Cerrahpaşa, Faculty of Engineering, Department of Chemistry, Istanbul, Türkiye
[2]Ataturk University, Faculty of Science, Department of Chemistry, Erzurum, Türkiye
[3]Marmara University, Faculty of Pharmacy, Department of Basic Pharmacy Sciences, İstanbul, Türkiye

Corresponding Author: Sinem Ortaboy E-mail ortaboy@iuc.edu.tr)

Received: 2024.10.17; Revised: 2024.10.22; Accepted: 2024.10.24

Abstract

Introduction: This study focused on synthesizing biocompatible, flexible and wearable electrode materials for energy storage applications. The unique zwitterionic structure of L-proline provides numerous interesting properties to the nanocomposite such as high ionic interactions through the various ion migration channels, and strong hydration characteristics. These features are key to the high performance of energy deposition systems.

Methods: Binary nanocomposites containing L-proline (Pro) amino acid and polypyrrole (Ppy) were produced on rGO modified carbon textile (rGO-CC) to develop electroactive materials. Two-step hydrothermal method was used to produce flexible electrodes. DRIFT spectroscopy and AFM analysis were performed to clarify the structural and the morphological characterization. Electrochemical behavior was evaluated utilizing CV, GCD and EIS methods.

Results: ProPpy@rGO-CC electrode materials exhibit high electrochemical performances in aqueous electrolytes (0.1 M NaCl). The prepared electrode shows high specific capacitance of 500.4 Fg^{-1} (at 25 mVs^{-1}) at the ambient conditions. Additionally, after 5,000 charge/discharge cycles the specific capacitance retains a high level of 95% confirming the good cycle stability. The energy and the power densities were found to be 278 Wh kg^{-1} and 12.5 kW kg^{-1}, respectively.

Conclusion: The results indicate that the ProPpy@rGO-CC electrode is a promising candidate for next-generation high-performance energy deposition systems. The unique structural features of L-proline contribute to the formation of a large number of electroactive sites and short diffusion pathways.

Keywords: Energy storage, amino acids, reduced graphene oxide, polypyrrole, supercapacitor

1. Introduction

Batteries and supercapacitors are critical components in modern renewable energy storage technologies. Particularly, supercapacitors have higher power density, long cycle life, and rapid charge-discharge characteristics when compared to the batteries. On one hand, recent advancements in supercapacitor technology have led to the

development of new materials and designs that improve their energy density, and making them more competitive with batteries. On the other hand, integrating supercapacitors with biological systems enhances bioenergy applications' performance. For example, wearable devices that harvest energy from human biofluids or movements can benefit from the rapid energy storage capabilities of supercapacitors. These devices can be utilized as biofuel cells to convert the biochemical energy into the electrical energy, which is then stored in supercapacitors for later use (1,2). This synergy not only enhances the efficiency of energy harvesting systems but also enables the development of self-powered wearable electronics (3).

Very recently, biological samples such as enzymes, amino acids, bacterial medium, etc. are extensively used as electrolyte materials or electrode active materials during the fabrication process of supercapacitor devices (4). Among biological systems, amino acid-based supercapacitors represent a promising area of research in energy storage technology. The utilization of amino acids as components in supercapacitors leverages their unique chemical properties, such as the presence of functional groups that can facilitate charge storage and enhance electrochemical performance. This approach not only contributes to the development of more efficient energy storage devices but also aligns with the growing demand for sustainable and biodegradable materials.

One of the primary advantages of using amino acids in supercapacitors is their ability to participate in protonation and deprotonation processes, which are essential for charge storage. Amino acids contain charged side chains, such as lysine, arginine, and glutamic acid that can undergo these reversible reactions, thus contributing to the capacitive charge storage mechanism. This characteristic is particularly beneficial for the design of ultrafast supercapacitors, where rapid charge and discharge cycles are crucial (5). Research has demonstrated that amino acids can serve as effective doping agents in the synthesis of carbon-based materials for supercapacitors. For instance, nitrogen-doped graphene hydrogels have been synthesized using amino acids, which not only improve the conductivity of the material but also enhance its electrochemical performance. The hydrothermal synthesis process allows the integration of amino acids into the graphene structure, resulting in materials with high surface areas and improved charge storage capabilities (6). Furthermore, amino acids can act as precursors for the production of nitrogen-doped carbon materials, which have shown significant promise in enhancing the performance of supercapacitors (7,8).

The development of amino acid ionic liquids (AAILs) has also opened new avenues for supercapacitor technology. AAILs exhibit favorable electrochemical properties, including high ionic conductivity and stability, making them suitable electrolytes for supercapacitors (9,10). Studies have shown that supercapacitors utilizing AAILs can achieve capacitance values comparable to those of conventional ionic liquid-based systems, thus demonstrating their viability as a sustainable alternative (9).

Moreover, the use of amino acids in the synthesis of metal-organic frameworks (MOFs) has been explored for their application in asymmetric supercapacitors. Amino-functionalized MOFs can provide high specific capacitance and serve as binder-free electrodes which simplifies the fabrication process and enhances the overall performance of the supercapacitor (11). This approach highlights the versatility of amino acids in creating advanced materials for energy storage applications. The unique properties of amino acids, such as their ability to participate in charge storage mechanisms and their vital role as precursors for advanced materials, make them as valuable components in the next generation of energy deposition systems. Ongoing research in this area is likely to give innovative approaches that meet both performance and environmental concerns in energy storage applications.

In the present study, an active electrode was synthesized using L-proline-derived conductive polymer on flexible textile substrates deposited with reduced graphene oxide (rGO). Hydrothermal method was applied to the synthesis of the active electrode composed of L-proline, and a

polypyrrole conductive polymer. The electrode obtained was evaluated electrochemically using cyclic voltammetry (CV), galvanostatic charge-discharge (GCD), and electrochemical impedance spectroscopy (EIS). The characterization of the electrode materials was performed diffuse reflectance infrared Fourier transform spectroscopy (DRIFT), Raman spectroscopy and atomic force microscopy (AFM) techniques.

2. Methods

2.1. Apparatus

Gamry 1010E Potentiostat/Galvanostat system (Gamry Instruments, Inc., Warminster, PA, USA) was used for all voltammetric measurements. Conventional three-electrode and two electrode systems were utilized in the investigation of electrode and supercapacitor performances, respectively. ProPpy@rGO-CC electrode (1x3 cm^2) served as the working electrode, a Ag/AgCl (3M KCl) electrode and Pt plate (0.5 cm^2) served as the reference and the counter electrode, respectively. The data was analyzed with an Echem Analyst 2 software interfaced with a computer (version 7.8.2). Carbon cloths (CC) were used as the flexible current collectors to produce ProPpy@rGO-CC electrode. The technical and mechanical properties of CC are given in Table 1.

Table 1. The technical and the mechanical properties of carbon cloth

The Technical and The Mechanical Properties of Carbon Cloth			
Weave	2/2 twill	**Tensile Modulus**	240 GPa
Weight	200 gm^{-2}	**Filament Diameter**	7 mm
Density	1.76 gcm^{-3}	**Elongation**	1.7 %
Dry fabric thickness	0.2 mm	**Fiber**	Carbon 3K
Tensile strength	3950 MPa	**Specific electrical resistance**	1.6 x 10^{-3} Wcm

Deionized water (DI) obtained from a Nüve water distillation system which was used throughout the experiments.

The electrochemical impedance spectroscopy (EIS) measurements were performed in the frequency range between 0.1 Hz and 100 kHz with an amplitude of superimposed alternative current (AC) signal of 10.0 mV at the open circuit potential (OCP).

The height asymmetries and nanostructural properties of the electrode surface were clarified by AFM, which was produced by Nanomagnetics-Instrument. It was operated in dynamic mode using aluminum coated silicon tips (PPP-NCLR, Nanosensors, Switzerland). The technical properties of the AFM tips were given in the following Table 2.

Table 2. The technical properties of the AFM tips

Property	**Nominal Value**	**Specified Range**
Resonance Frequency [kHz]	190	146 - 236
Force Constant [N/m]	48	21 – 98
Length [µm]	225	215 - 235
Mean Width [µm]	38	30 – 45
Thickness [µm]	7	6 – 8

Samples were recorded with the scanning rate of 5 μms^{-1} and 256 × 256 pixels resolution to obtain a view of 5 × 5 μm^2 area. The AFM images were evaluated using the "NMI Viewer 2.0.7. Image Analyzer" software. Diffuse Reflectance Infrared Fourier Transform Spectroscopy (DRIFT) techniques were applied for the chemical characterization of active electrode materials. The DRIFT spectra were obtained using Bruker-Alpha T model spectrophotometer. Mass ratio of active electrode material to KBr was kept constant at 1/150 (*w*/*w*). All electrochemical experiments were performed at room temperature (25 ± 2 °C, 54% humidity)

2.2. Preparation of ProPpy@rGO-CC electrodes

The modified Hummer's method was adopted to produce graphene oxide (GO). Hence, 0.5 g of graphite powder and 3 g of $KMnO_4$ were mixed in a mortar and pestle. H_2SO_4 and H_3PO_4 mixture in the ratio of 9:1 was added to the powder mixture with continuous magnetic stirring. The greenish black solution was obtained. Then, the heating process was applied to the solution (60 °C - 24 h) until the color of solution turned to brown color. The dropwise addition of H_2O_2 (30%) was carried out in an ice bath. After the yellow color was seen,

the product was washed thoroughly with DI water and ethanol followed by the drying at 55 °C. Then, hydrothermal synthesis was used to fabricate rGO-CC. Firstly, suspension of 50 mg of as-synthesized GO in 25 mL of ethylene glycol were prepared by sonication during 30 min. The resulted colloidal solution turned to brown color. The mixture was poured into the Teflon-lined autoclave for 12 hours keeping at 150 °C. At the same time, the textile substrate in the dimension 3x1 cm^2 was placed in to the autoclave. After the hydrothermal process the rGO-CC electrode washed thoroughly with acetone and DI water. Finally, it was dried in an oven at 55 °C overnight. L-proline solution in ethanol, pyrrole, and $(NH_4)_2S_2O_8$ were mixed in an ultrasonic bath. The mix solution and the rGO-CC was transferred to the sealed Teflon lined autoclave and was placed at 120 °C for 12 hours in a furnace. The resulting electrode was cleaned and dried applying the same procedure as mentioned above. The electrode obtained was named as ProPpy@rGO-CC.

3. Result and Discussion

3.1. Structural Characterizations

Fig 1 shows the Raman spectra of GO powder and rGO films hydrothermally deposited on the textile substrate. The typical prominent bands observed at ~1600 cm^{-1} (G band) and at ~1345 cm^{-1} (D band), caused by E_{2g} mode (sp^2 carbon) in graphene and breathing mode of aromatic moieties were clarified (12). Additionally, the weak broad bands located at about 2690, 2940 and 3180 cm^{-1} also identified from the spectra (2D band). The intensity ratio of D bands and G bands (I_D/I_G) gives the critical information about defect regions of carbon lattice. The ratio of I_D/I_G increases in the presence of rGO in the structure due to the transformation and enhanced disorder following chemical reduction (13). This trend corresponds to the findings obtained from the present study. The I_D/I_G ratios are found as 0.96 and 1.13 for GO and rGO, respectively.

Furthermore, the 2D band, also provides an important aspect regarding the number of graphene layers and the electronic structure of the material. In rGO, the 2D band generally exhibits a shift towards lower wavenumbers compared to GO, which can be attributed to changes in the electronic environment and the reduction in the number of layers (14,15). In this study, the 2D bands in rGO located about 20 cm^{-1} wavenumbers less when compared to those of GO bands confirming the formation of rGO.

Fig 2 presents the DRIFT spectrum of ProPpy@rGO-CC electrode. In the spectrum the peaks observed at 822 and 1030 cm^{-1} were ascribed to PPy structure, whereas the peaks at 3326, 2935, 1727, 1517, 1393, 1251, and 1098 cm^{-1} are assigned to N-H, C-H (sp^3), C=O, C–N, C=C (backbone stretching), N-O, C–O, and C–C stretching, respectively, describing the characteristics of PPy and L-proline (16). The peak observed at 1517 cm^{-1} is attributed to the carboxyl group of GO.

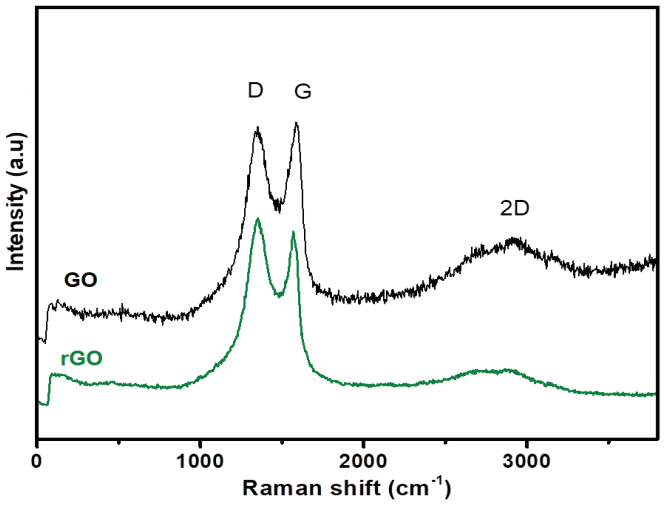

Figure 1. Raman spectra of GO powder and rGO film deposited onto CC substrate

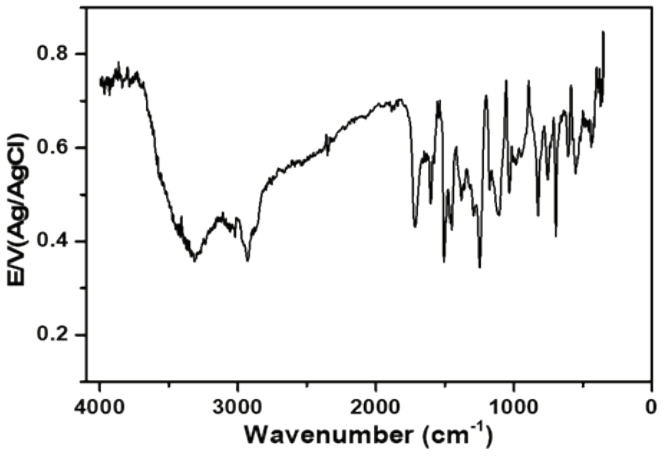

Figure 2. DRIFT spectrum of ProPpy@rGO film on textile substrate

Polypyrrole exhibits significant interactions with amino acids, which can be leveraged in various

applications, including biosensors, energy and drug delivery systems due to the unique chemical structure of both polypyrrole and the amino acid moieties. In this study, one of the primary mechanisms of interaction between polypyrrole and L-proline is electrostatic attraction. Oxidized polypyrrole, which carries anionic charges, enhances its affinity for L-proline allowing for selective binding based on charge interactions (17). Additionally, it was proposed that L-proline can interact with polypyrrole through multiple bonding mechanisms involving electrostatic, hydrogen bonding, and covalent interactions. These interactions not only influence the binding affinity of amino acids to polypyrrole but also enhance the functional properties of the polymer for various applications in materials, science and biochemistry (18,19). The role of amino acids in modulating the properties of polypyrrole is also significant. For example, the incorporation of amino acids can alter the electrochemical properties of polypyrrole, enhancing its conductivity and stability, which is crucial for applications in energy and biosensing (17). Furthermore, π-π interactions and hydrogen bonding between the rGO layers and aromatic rings of PP and L-proline also play an important role in the formation of hybrid nanocomposites (20). The proposed interaction mechanism is shown in the following illustration (Fig 3).

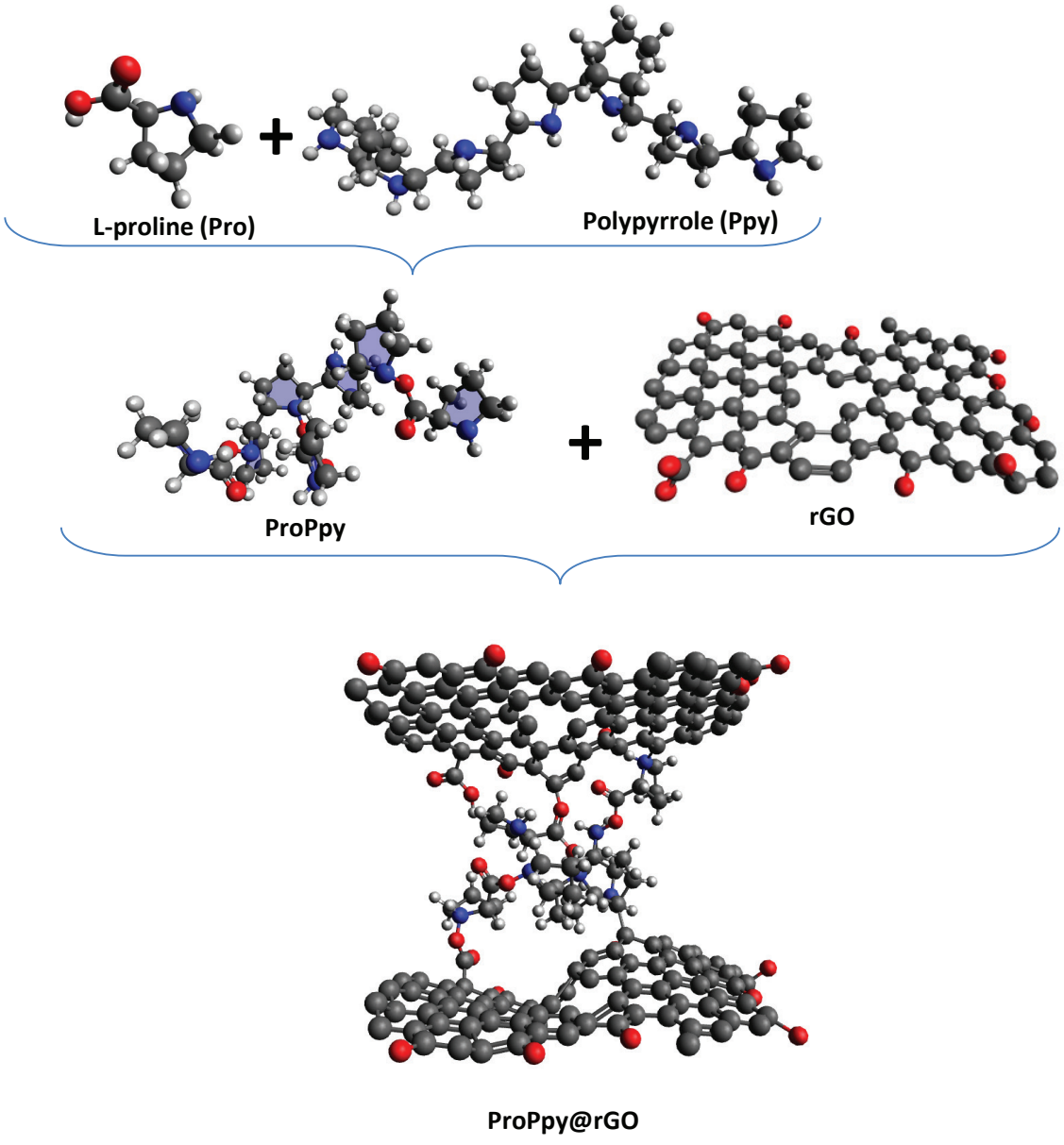

Figure 3. Schematic illustration of reaction mechanisms of ProPpy@rGO deposited on textile substrate.

3.2. Morphological Characterizations

The morphological characterization of the ProPpy@rGO-CC electrode was investigated via the AFM technique. The phase images provide insights into the mechanical properties and structural variations within the composite materials, which are crucial for understanding their performance in various applications. Phase separation can lead to distinct regions within the composite, affecting its electrical and mechanical properties. Moreover, the morphology of polypyrrole composites can be influenced by the presence of L-Proline and rGO. It is well known that phase separation can significantly alter the electrical conductivity of the materials (21,22). Fig 4 exhibits the detailed phase profiles of the ProPpy@rGO-CC electrode. According to Fig 4, the film dimensions investigated are approximately 5x5 μm^2.

Depending on their unique properties, such as surface energy and modulus, the bright regions show the hard segments, while the dark areas indicate the soft segments of the electrode material (23,24). As shown in Fig 4a and 4c, the polymeric structures, L-proline, and rGO are evenly distributed in the matrix. The histogram profile revealed positive phase shifts relative to the 90° phase shift observed at resonance, implying that a repulsive force is effective between the tip and the sample surface for investigated segments. Additionally, the cross-section profile obtained from the linear line on the 2D phase image shows the phase distribution fluctuated between 5-20° for different segments.

3.3. Electrochemical Characterization of *ProPpy@rGO-CC* Electrodes

Electrochemical performance of ProPpy@rGO-CC electrode was evaluated using cyclic voltammetry (CV), galvanostatic charge-discharge (GCD) and electrochemical impedance spectroscopy (EIS) techniques. CV analysis was performed at a potential window of -1.0 V – 1.0 V with various scan rates from 0.005 Vs^{-1} to 0.5 Vs^{-1}. 0.1 M NaCl aqueous solution was served as an electrolyte to

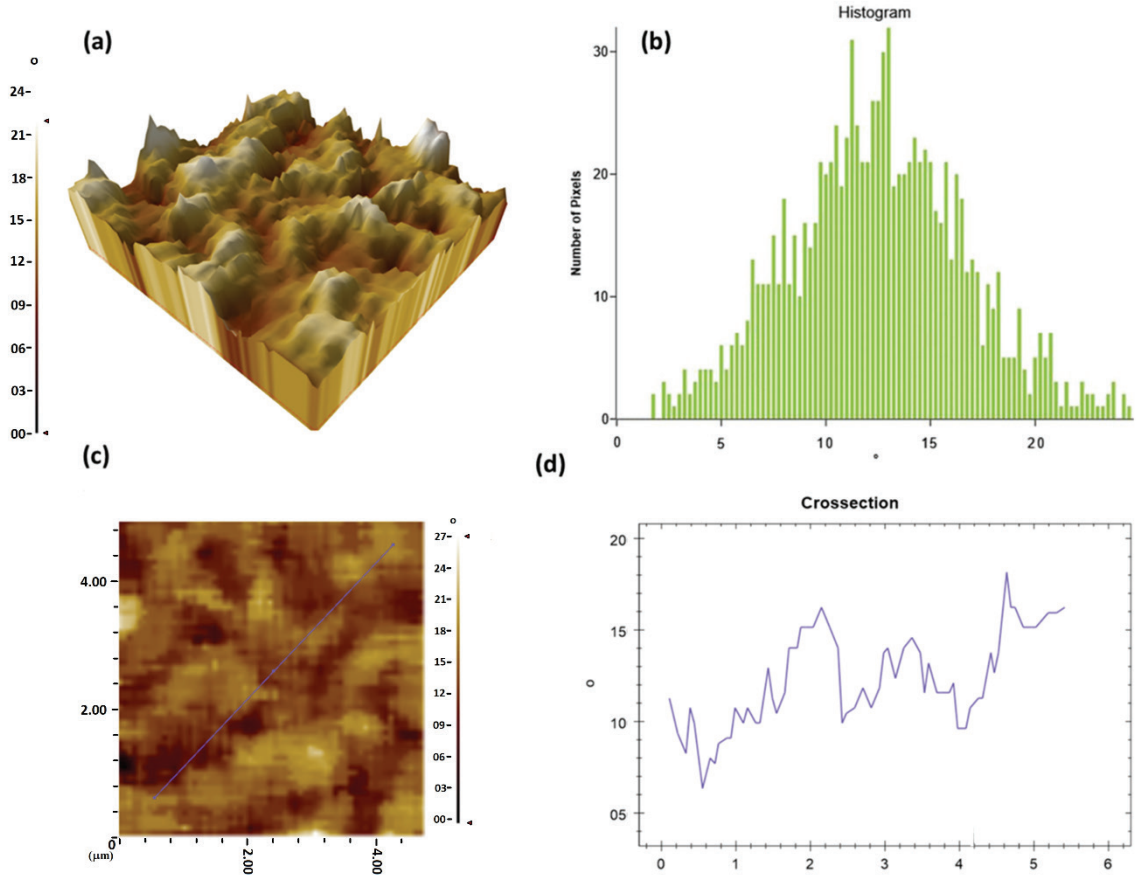

Figure 4. AFM phase images of the ProPpy@rGO-CC electrode, **a)** 3D view, **b)** the phase distribution histogram curve, **c)** 2D view and crossectional line, **d)** the phase changes through the crossectional line.

provide biocompatible medium for biological applications. The specific capacitance C (Fcm^{-2}) of the film electrode was determined by means of cyclic voltammetry (CV) according to the following equation.

$$C = \int \frac{IdV}{A\vartheta(\Delta V)} \quad (1)$$

Where ΔV is the potential window, ΔV = (V_{final} - $V_{initial}$), A is the active surface area of the electrode (cm^{-2}), I is the responsive current (A), and υ is the scan rate (Vs^{-1}).

The CV curves of ProPpy@rGO-CC electrode shows a faradic nature as shown in Fig 5a. At relatively low scan rate (25 mVs^{-1}) well-defined reversible redox peaks were observed which indicate that a pseudo-capacitive behavior based on a redox (faradaic) mechanism is effective. Both the increase in maximum peak currents and the shift of the oxidation/reduction peak potentials towards higher and lower overpotentials further indicate that the prepared electrode possesses desirable electrochemical properties such as enhanced interaction at electrode/electrolyte surface, high surface area and good electrical conductivity (25). The peak separations as a function of scan rates is given in Fig 5a inset.

For further characterization, galvanostatic charge discharge curves were measured at different current densities with potentials between -1.0 V – 1.0 V (Fig 5b). To observe the complete reaction between the electrode and the electrolyte interface, relatively

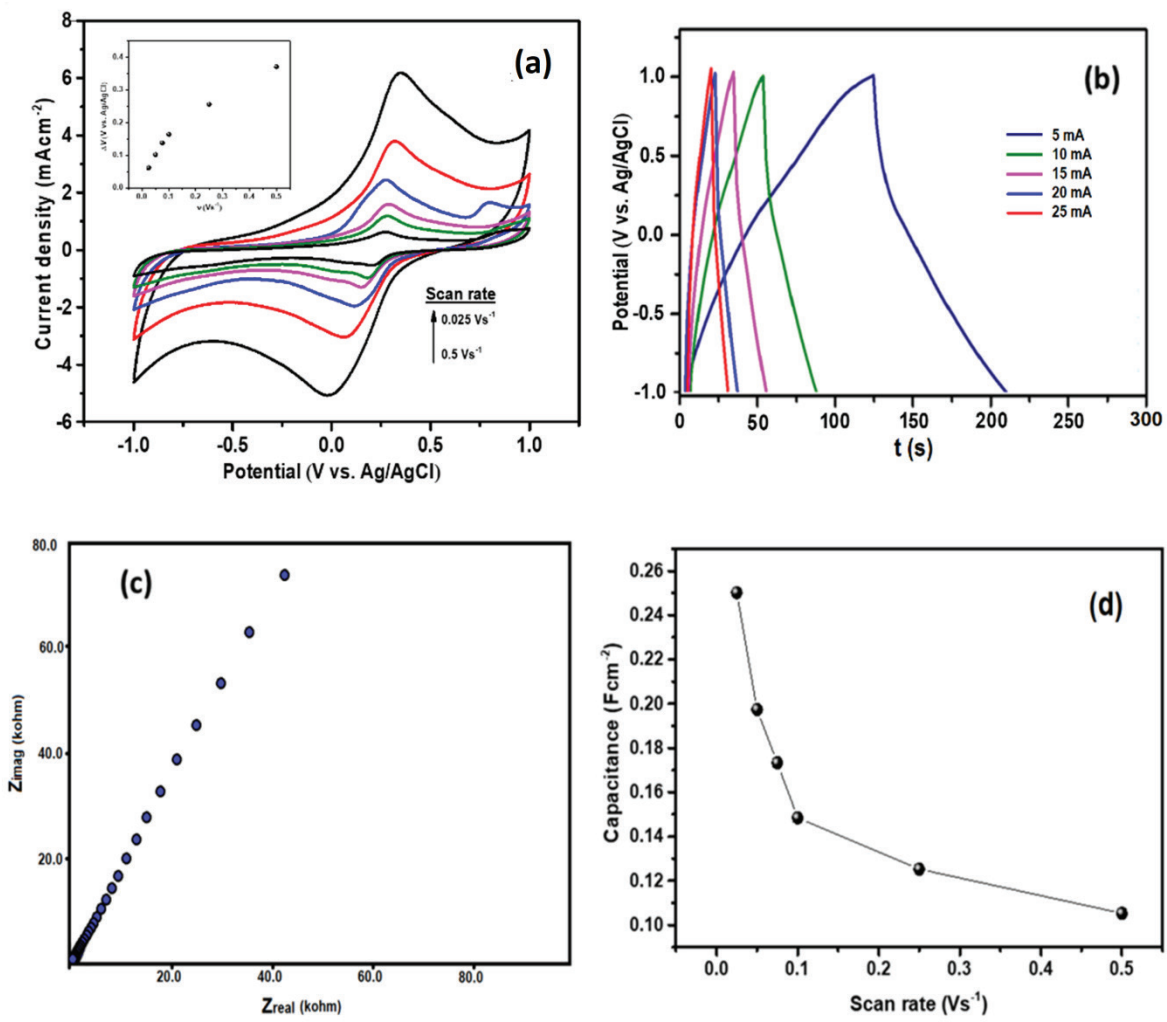

Figure 5. a) Cyclic voltammograms with various scan rates, **b)** galvanostatic charge-discharge curves with various current, **c)** electrochemical impedance spectroscopy (0.01 Hz-100 kHz frequency, 10 mV amplitude), **d)** the change of the capacitance values as a function of scan rates for the ProPpy@rGO-CC electrode in aqueous 0.5 M NaCl electrolyte.

low current density (5 $mAcm^{-2}$) was applied. For ProPpy@rGO-CC hybrid electrode, the calculated specific capacitance values were 500.4, 394.8, 346.5, 322.1, 250.6, and 210.7 Fg^{-1} at the current densities of 5, 10, 15, 20, and 25, Ag^{-1}, respectively. From the results, it is observed that with increasing current density the discharge time gets lower indicating that the faradaic reaction is a diffusion-controlled process occurring at the material surface.

Electrochemical Impedance Spectroscopy (EIS) is a significant technique used to evaluate and understand the electrical resistance and its related phenomenon. EIS measurements were performed in a frequency range between 100 kHz and 0.01 Hz at open circuit potential (OCP) with an alternating current perturbation of 10 mV. The Nyquist plot of the electrode is shown in Fig 5c. The plot exhibits a linear line in the low frequency region, related to the Warburg impedance, indicating the good electron transfer behavior. In the high frequency region, no semicircle was observed, showing that the charge transfer process increases in the supporting electrolyte during the charging and discharging periods (26). The solution resistance of the electrode was observed at approximately 3 ohm. It is well known that in the presence of rGO, the good electrical conductivity allows to decrease the resistance of charge transfer in the electrode/electrolyte interface. Fig 5d shows the change of areal capacitance as a function of increasing scan rates.

Capacitance retention against number of cycles is an important parameter to evaluate the electrochemical performance for practical energy storage applications. As it is seen from the Fig 6a, the ProPpy@rGO-CC electrode shows 95.4% capacitance retention after 5000 consecutive CV cycles recorded at a scan rate of 2 Vs^{-1}. Fig 6b exhibits Ragone plot which is utilized to compare the performance characteristics of different electrode materials prepared for energy storage devices.

The following equations were used to calculate energy and power densities by using cyclic voltammetry results (27).

$$E = \frac{1}{2} C(\Delta V)^2 \quad (2)$$

$$P = \frac{E}{t} \quad (3)$$

where C is the specific (or areal) capacitance, ΔV is the voltage window, P is the power density, t is the discharge time.

According to these equations, maximum specific energy and specific power were calculated as 278.1 Wh kg^{-1} (139.2 μWhcm^{-2}) and of 12.5 kW kg^{-1} (52.7 mWhcm^{-2}), respectively. These results are superior to those of previously published electrode materials, such as CQD-/Ppy-N (0,06 Whcm^{-2} at 8.4 W cm^{-2}) (28); GO/PPy (0.01 Whcm^{-2} at 0.1 Wcm^{-2}) (29); RGO (0.2 mWhcm^{-2} at 50 Wcm^{-2}) (30); nitrogen and sulfur co-doped porous carbon fibers film (N, S

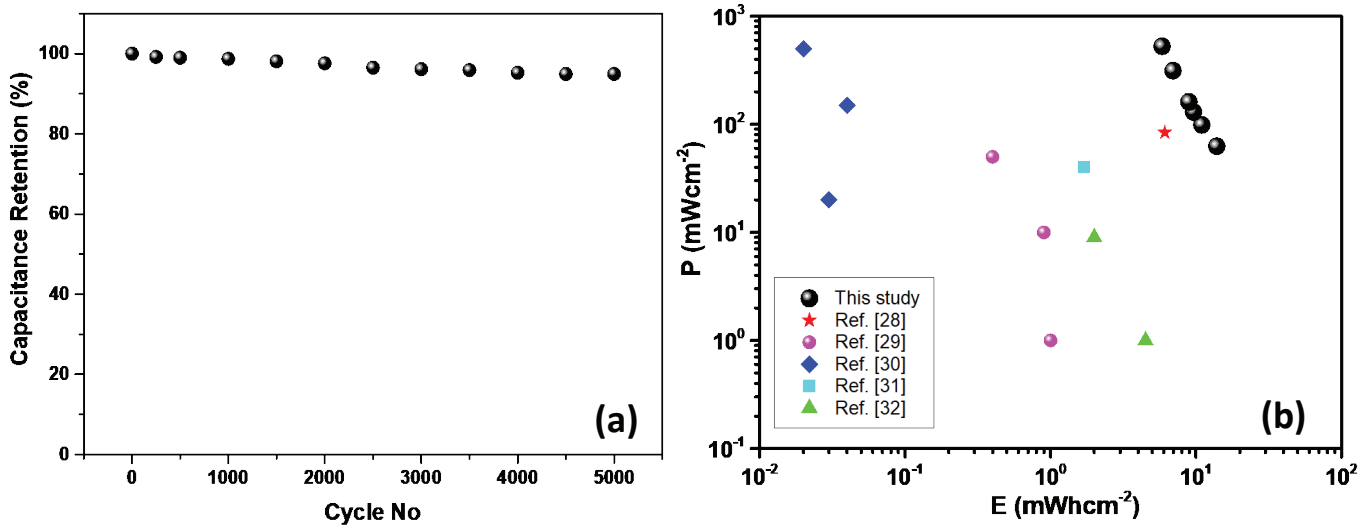

Figure 6. a) Capacitance retention of ProPpy@rGO-CC electrode for 5000 cycles at a scan rate of 2.0 Vs^{-1}, **b)** Areal Ragone plot showing areal energy and power densities of various electrodes for energy storage systems.

co-doped PCFF) (0.02 $Whcm^{-2}$ at 4 Wcm^{-2}) (31) and graphene/polypyrrole aerogel (GPA) (0.04 $Whcm^{-2}$ at 0.1 Wcm^{-2}) (32).

4. Conclusion

In summary, we have successfully synthesized ProPpy@rGO-CC flexible electrode by using simple two-step hydrothermal method. The morphological and chemical characterization of electrode was clarified by using DRIFTS and AFM techniques. The synthesized ProPpy@rGO-CC electrode showed a maximum specific capacitance of 500.4 Fg^{-1} (215.0 $mFcm^{-2}$), high specific energy of 278.1 Wh kg^{-1} (139.2 $\mu Whcm^{-2}$), and specific power of 12.5 kW kg^{-1} (52.7 $mWhcm^{-2}$). It is observed that the electrode maintains its initial capacity of 95.4% after 5000 cycles confirming long time cyclic stability at a scan rate of 2.0 Vs^{-1}. The remarkable electrochemical performance can be attributed to the synergistic effect among L-Proline, PPy, and rGO moieties, resulting in abundant electroactive sites and fast diffusion pathways.

Conflicts of interest: The authors report no conflicts of interest.

References

1. Guan S, Li J, Wang Y, Yang Y, Zhu X, Ye D, Liao Q. Multifunctional MOF-derived Au, Co-doped porous carbon electrode for a wearable sweat energy harvesting–storage hybrid system. Adv Mater. 2023;35(39). doi:10.1002/adma.202304465
2. Lv J, Chen J, Lee PS. Sustainable wearable energy storage devices self-charged by human-body bioenergy. SusMat. 2021;1(2):285-302. doi:10.1002/sus2.14
3. Yin Y, Yang C, Li M, Zheng Y, Ge C, Gu J, Li H, Duan M, Wang X, Chen R. Research progress and prospects for using biochar to mitigate greenhouse gas emissions during composting: a review. Sci Total Environ. 2021;798. doi:10.1016/j.scitotenv.2021.149294
4. Ahmed S, Sharma P, Bairagi S, Rumjit NP, Garg S, Ali A, Lai CW, Mousavi SM, Hashemi, SA, Hussain CM. Nature-derived polymers and their composites for energy depository applications in batteries and supercapacitors: Advances, prospects and sustainability. J. Energy Storage. 2023;66:107391. doi:10.1016/j.est.2023.107391
5. Mosa IM. Biosupercapacitors for Implantable Bioelectronics & Portable Microfluidic Devices for Prostate Cancer Biomarker Detection and DNA Damage Screening. 2018.
6. Wang T, Wang L, Wu D, Xia W, Zhao H, Jia D. Hydrothermal synthesis of nitrogen-doped graphene hydrogels using amino acids with different acidities as doping agents. J. Mater. Chem. A. 2014;2(22):8352-8361. doi:10.1039/C4TA00170B
7. Ma G, Yang Q, Sun K, Peng H, Ran F, Zhao X, Lei Z. Nitrogen-doped porous carbon derived from biomass waste for high-performance supercapacitor. Bioresour Technol. 2015;197:137-142. doi:10.1016/j.biortech.2015.07.100
8. Fu X, Li R, Yan S, Yuan W, Zhang Y, Sun W, Wang X. Porous carbons prepared from polyacrylonitrile doped with graphitic carbon nitride or melamine for supercapacitor applications. ChemistrySelect. 2023;8(34). doi:10.1002/slct.202301801
9. Wu M, Li W, Li S, Feng G. Capacitive performance of amino acid ionic liquid electrolyte-based supercapacitors by molecular dynamics simulation. RSC advances. 2017;7(46):28945-28950. doi:10.1039/C7RA00443E
10. Zhou H, Zhou Y, Li L, Li Y, Liu X, Zhao P, Gao B. Amino acid protic ionic liquids: multifunctional carbon precursor for N/S codoped hierarchically porous carbon materials toward supercapacitive energy storage. ACS Sustainable Chem. Eng. 2019;7(10):9281-9290. doi:10.1021/acssuschemeng.9b00279
11. Sun J, Yu X, Zhao S, Che H, Tao K, Han L. Solvent-controlled morphology of amino-functionalized bimetal metal–organic frameworks for asymmetric supercapacitors. Inorg Chem. 2020;59(16):11385-11395. doi:10.1021/acs.inorgchem.0c01157
12. Stankovich S, Dikin DA, Piner RD, Kohlhaas KA, Kleinhammes A, Jia Y, Wu Y, Nguyen ST, RodRuoff RS, Synthesis of graphene-based nanosheets via chemical reduction of exfoliated graphite oxide. Carbon. 2007;45(7):1558-1565. doi:10.1016/j.carbon.2007.02.034

13. Kang Y, Li W, Ma T, Huang X, Mo Y, Chu Z, Zhang Z, Feng G. Microwave-constructed honeycomb architectures of h-BN/rGO nano-hybrids for efficient microwave conversion. Compos. Sci. Technol. 2019;174:184-193. doi:10.1016/j.compscitech.2019.02.029

14. Shahid M, Katugampalage TR, Khalid M, Ahmed W, Kaewsaneha C, Sreearunothai P, Opaprakasit P. Microwave assisted synthesis of Mn3O4 nanograins intercalated into reduced graphene oxide layers as cathode material for alternative clean power generation energy device. Sci Rep. 2022;12(1). doi:10.1038/s41598-022-23622-x

15. Sabari Girisun TC, Saravanan M, Soma VR. Wavelength-dependent nonlinear optical absorption and broadband optical limiting in Au-Fe2O3-rGO nanocomposites. ACS Appl. Nano Mater. 2018;1(11). doi:10.1021/acsanm.8b01544

16. Schoustra S, Kloots M, Posthuma J, Doorn D, Dijksman J, Smulders M. Raman spectroscopy reveals phase separation in imine-based covalent adaptable networks. Macromolecules. 2022;55(23), doi:10341-10355

17. Chen Z, Takei Y, Deore BA, Nagaoka T. Enantioselective uptake of amino acid with overoxidized polypyrrole colloid templated with l-lactate. Analyst. 2000;125(12):2249-2254. doi:10.1039/b005745m

18. Dipojono H, Safitri I, Budi E, Saputro A, David M, Kasai H. Immobilization of amino acids leucine and glycine on polypyrrole for biosensor applications: a density functional theory study. Itbj Eng Sci. 2011;43(2),113-122. doi:10.5614/itbj.sci.2011.43.2.4

19. Azioune, A, Chehimi, M, Miksa, B., Basiǹska, T, Słomkowski, S. Hydrophobic protein−polypyrrole interactions: the role of van der waals and lewis acid−base forces as determined by contact angle measurements. Langmuir. 2002;18(4:1150-1156. doi:10.1021/la010444o

20. Zhu C, Zhai J, Wen D, Dong S. Graphene oxide/polypyrrole nanocomposites: one-step electrochemical doping, coating and synergistic effect for energy storage. J. Mater. Chem. 2012;22: 6300. doi:10.1039/c2jm16699b

21. Vleminckx G, Bose S, Leys J, Vermant J, Wübbenhorst M, Abdala A, Macosko C, Moldenaers P. Effect of thermally reduced graphene sheets on the phase behavior, morphology, and electrical conductivity in poly[(α-methyl styrene)-co-(acrylo,nitrile)/poly(methyl-methacrylate) blends. ACS Appl. Mater. Interfaces. 2011;3(8):3172-3180. doi:10.1021/am200669w

22. Bose S, Özdilek C, Seo J, Wübbenhorst M, Vermant J, Moldenaers P. Phase separation as a tool to control dispersion of multiwall carbon nanotubes in polymeric blends. ACS Appl. Mater. Interfaces. 2010;2(3):800-807. doi:10.1021/am9008067

23. Butt HJ, Cappella B, Kappl M. Force measurements with the atomic force microscope: Technique, interpretation and applications. J. Surf. Rep. 2005;59(1-6):1-152. doi:10.1016/j.surfrep.2005.08.003

24. Schirmeisen A, Anczykowski B, Fuchs H. Dynamic modes of atomic force microscopy. In: Bhushan B, editor. Springer handbook of nanotechnology. Berlin, Heidelberg: Springer; 2007. p 27. doi:10.1007/978-3-540-29857-1_27

25. Veeramani V, Madhu R, Chen SM, Sivakumar M, Hung CT, Miyamoto N, Liu SB, NiCo2O4-decorated porous carbon nanosheets for high-performance supercapacitors. J. Electacta. 2017;247:288-295. doi:10.1016/j.electacta.2017.06.171

26. Britto S, Ramasamy V, Murugesan P, Thangappan R, Kumar R. Preparation and electrochemical validation of rGO-TiO2-MoO3 ternary nanocomposite for efficient supercapacitor electrode. Diamond Relat. Mater. 2022;122:108798. doi:10.1016/j.diamond.2021.108798

27. Ortaboy S, Alper JP, Rossi F, Bertoni G, Salviati G, Carraro C, Maboudian R. MnOx-decorated carbonized porous silicon nanowire electrodes for high performance supercapacitors. Energy Environ. Sci. 2017;10(6):1505-1516. doi:10.1039/C7EE00977A

28. Jian X, Li JG, Yang HM, Zhang EH, Liang ZH. Carbon quantum dots reinforced polypyrrole nanowire via electrostatic self-assembly strategy for high-performance supercapacitors. Carbon. 2017;114:533-543, doi:10.1016/j.carbon.2016.12.033

29. Cao J, Wang Y, Chen J, Li X, Walsh FC, Ouyang J, Jia D, Zhou Y. Three-dimensional graphene oxide/polypyrrole composite electrodes fabricated by one-step electrodeposition for high performance supercapacitors, J. Mater. Chem. A, 2015;3:14445-14457. doi:10.1039/C5TA02920A

30. Yang C, Zhang L, Hu N, Yang Z, Wei H, Zhang Y. Reduced graphene oxide/polypyrrole nanotube papers for flexible all-solid-state supercapacitors with excellent rate capability and high energy density. J. Power Sources. 2016;302:39-45. doi:10.1016/j.jpowsour.2015.10.035

31. Chen L, Wen Z, Chen L, Wang W, Ai Q, Hou G, Li Y, Lou J, Ci L. Nitrogen and sulfur co-doped porous carbon fibers film for flexible symmetric all-solid-state supercapacitors. Carbon. 2020;158:456-464. doi:10.1016/j.carbon.2019.11.012

32. Ye S, Feng J. Self-assembled three-dimensional hierarchical graphene/polypyrrole nanotube hybrid aerogel and its application for supercapacitors. ACS Appl. Mater. Interfaces. 2014;6(12):9671-9679 doi:10.1021/am502077p

Cite this article: Ortaboy S, Ogretici M, Aras K, Salihi Caliskan E. Amino Acid Supported Conductive Nanocomposite for Developing Flexible Electrode Material for Energy Storage. Pharmedicine J. 2024;1(3), 110-120. DOI: 10.62482/pmj.16